Forschungszentrum Karlsruhe
Technik und Umwelt

Wissenschaftliche Berichte
FZKA 6263

Features of the EAS Muon Density Distributions measured with the KASCADE Experiment

A. Haungs, K. U. Köhler, H. Leibrock, H. Rebel, T. Antoni, W. D. Apel, A. F. Badea, K. Bekk, K. Bernlöhr, E. Bollmann, H. Bozdog, I. M. Brancus, A. Chilingarian, K. Daumiller, P. Doll, J. Engler, F. Feßler, H. J. Gils, R. Glasstetter, R. Haeusler, W. Hafemann, D. Heck, T. Holst, J. R. Hörandel, K. H. Kampert, H. Keim, J. Kempa, H. O. Klages, J. Knapp, H. J. Mathes, H. J. Mayer, J. Milke, D. Mühlenberg, J. Oehlschläger, M. Petcu, M. Risse, M. Roth, G. Schatz, H. Schieler, F. K. Schmidt, T. Thouw, H. Ulrich, A. Vardanyan, B. Vulpescu, J. H. Weber, J. Wentz, T. Wibig, T. Wiegert, D. Wochele, J. Wochele, J. Zabierowski, S. Zagromski

Institut für Kernphysik

Februar 1999

Forschungszentrum Karlsruhe

Technik und Umwelt

Wissenschaftliche Berichte

FZKA 6263

Features of the EAS Muon Density Distributions measured with the KASCADE Experiment

A. Haungs, K.U. Köhler, H. Leibrock, H. Rebel,
T. Antoni, W.D. Apel, A.F. Badea[1], K. Bekk, K. Bernlöhr,
E. Bollmann, H. Bozdog[1], I.M. Brancus[1], A. Chilingarian[2],
K. Daumiller[3], P. Doll, J. Engler, F. Feßler, H.J. Gils,
R. Glasstetter, R. Haeusler, W. Hafemann, D. Heck,
T. Holst, J.R. Hörandel, K.H. Kampert, H. Keim,
J. Kempa[4], H.O. Klages, J. Knapp[3*], H.J. Mathes,
H.J. Mayer, J. Milke, D. Mühlenberg, J. Oehlschläger,
M. Petcu[1], M. Risse, M. Roth, G. Schatz, H. Schieler,
F.K. Schmidt[3], T. Thouw, H. Ulrich, A. Vardanyan[2],
B. Vulpescu[1], J.H. Weber, J. Wentz, T. Wibig[4], T. Wiegert,
D. Wochele, J. Wochele, J. Zabierowski[5], S. Zagromski

Institut für Kernphysik

[1]Institute of Physics and Nuclear Engineering, Bucharest, Romania
[2]Cosmic Ray Division, Yerevan Physics Institute, Yerevan, Armenia
[3]Institut für Experimentelle Kernphysik, Univ. Karlsruhe, Germany
[4]Department of Experimental Physics, Univ. Lodz, Lodz, Poland
[5]Soltan Institute for Nuclear Studies, Lodz, Poland

[*]Now at: University of Leeds, Leeds, U.K.

Forschungszentrum Karlsruhe GmbH, Karlsruhe
1999

Forschungszentrum Karlsruhe GmbH
Postfach 3640, 76021 Karlsruhe

Mitglied der Hermann von Helmholtz-Gemeinschaft
Deutscher Forschungszentren (HGF)

ISSN 0947-8620

Abstract

Using the KASCADE detector measurements of the EAS muon density and its fluctuations have been performed at two different thresholds of muon energy. The results are classified according to the EAS size N_e and the energy indicating parameter N_μ^{tr}. Average lateral muon density distributions have been determined. The observed features are studied in context of CORSIKA simulations, based on different models of the high-energy hadronic interaction. In particular, signatures of the knee in the primary spectrum and the sensitivity to the mass composition have been investigated. An interesting result of special importance is the first observation of kinks in muon density spectra, measured at fixed distances from the EAS center. They indicate the knee phenomenon and are analysed in terms of the knee position and the slopes of the primary spectrum.

Zusammenfassung

Myondichte-Untersuchungen von ausgedehnten Luftschauern im KASCADE Experiment

Mit Hilfe des KASCADE-Detektorsystems wurden Messungen der EAS-Myondichte und deren Fluktuationen bei zwei verschiedenen Nachweisschwellen der Myonenergie durchgeführt. Die Resultate wurden klassifiziert nach Schauergröße N_e, bzw. nach dem energieproportionalen Parameter N_μ^{tr}, und gemittelte Lateralverteilungen der EAS-Myondichte wurden bestimmt. Die beobachteten Eigenschaften, insbesondere Signaturen auf das "Knie" im Primärspektrum und die Empfindlichkeit auf die Massenzusammensetzung der primären kosmischen Strahlung wurden im Zusammenhang mit CORSIKA-Simulationen auf der Basis verschiedener Modelle der hochenergetischen hadronischen Wechselwirkung untersucht. Ein interessantes Ergebnis von spezieller Bedeutung ist die erstmalige Beobachtung von abrupten Änderungen im Abfall ("kinks") der Myondichte-Spektren (gemessen bei festen Abständen vom Schauerzentrum), die das Knie-Phänomen reflektieren. Diese Myondichte-Spektren werden mit Hilfe von CORSIKA-Simulationen hinsichtlich des Verlaufs und der Position des Knies des Primärspektrums analysiert.

Contents

1 Introduction

For forty years a conspicuous change of the spectral index from ca. -2.7 to -3.1 of the power law description of the primary cosmic ray spectrum around 3 PeV is known [1]. This knee has been found by measurements of the charged particle size spectra in observations of Extensive Air Showers (EAS) and was furtheron confirmed, see ref. [2] for a review. In spite of a lot of experimental efforts, there remain many open questions, in particular about the detailed position and the shape of the knee region, about the variation of the primary mass composition, in addition to the question of the astrophysical origin of the observed features at all. There is a number of theoretical conjectures about the mass composition, predicting a variation from dominantly light nuclei (with a proton and helium fraction of about 65% as observed in direct experiments with satellite and balloon borne detectors [3]) to a composition of heavier nuclei.

The approach of the KASCADE experiment [4, 5], focussed on a determination of the energy spectrum and mass composition of primary cosmic rays, is guided by a simultaneous event-by-event observation of many different EAS parameters of the electron-photon, muon and hadron components with a detector array of a larger degree of sampling and by a correlation analysis of various signatures of the primary mass on basis of Monte Carlo simulations using advanced hadronic interaction models. Apart from observational inaccuracies the main difficulties of inference of the energy and nature of the primary particle originate from the intrinsic fluctuations of the EAS development in the atmosphere. On the way towards a better understanding of these features and of the basic information potential of the EAS parameters, a detailed study of the average characteristics is indispensable. In particular, a consideration of the penetrating muon component is expected to be a source of relatively undistorted information about the early EAS stages.

In this paper we report on detailed experimental studies of the mean lateral distribution and the fluctuations of the local density of the EAS muon component, observed with the muon detection facilities of the KASCADE setup at two different muon energy detection thresholds (250 MeV and 2 GeV, respectively). Local muon density spectra at fixed distances from the shower axis have been measured and display conspicuous kinks at certain values of the local muon density. The analysis of this observation by use of extensive Monte Carlo EAS simulation calculations relates the observed kinks to the knee of the primary cosmic ray energy spectrum and implies new methodical aspects of EAS investigations.

2 Experimental Setup and Procedures

The KASCADE detector array [4] consists of a detector field having an area of $200 \times 200\,\mathrm{m}^2$ and 252 detector stations (positioned on rectangular grids with 13 m spacing), of the central detector comprising various different detection facilities and a limited streamer-tubes setup in a tunnel, at present partly in operation. The present measurements of the muon component use the muon detectors of the field array and the multiwire proportional chambers (MWPC) of the central detector. The field array, which also provides the general EAS trigger and the data necessary for the reconstruction of the basic EAS characteristics (size, core location and angle of incidence) is built up of 16 autonomous clusters, the outer 12 clusters comprising 16 stations each and the central four clusters 15 stations (see Figure 1).
Figure 2 displays a schematic layout of a detector station. For the electron-photon detection there is a liquid scintillator in stainless steel containers of 100 cm diameter with a photomultiplier on the top. The container is filled with argon to prevent oxidation of the scintillator material. The 12 clusters in the outer region of the field contain two of such electron-photon detectors, positioned in the diagonal of each station. The inner four clusters contain four of such detectors for each station. The

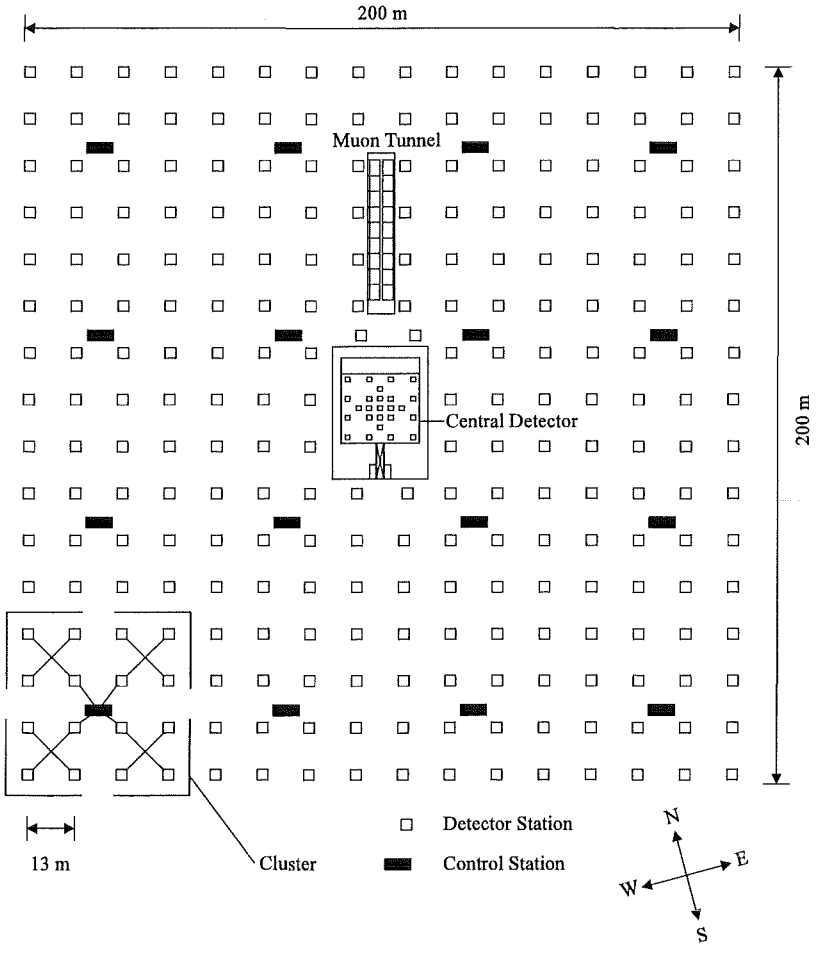

Figure 1: *Schematic layout of the KASCADE Experiment.*

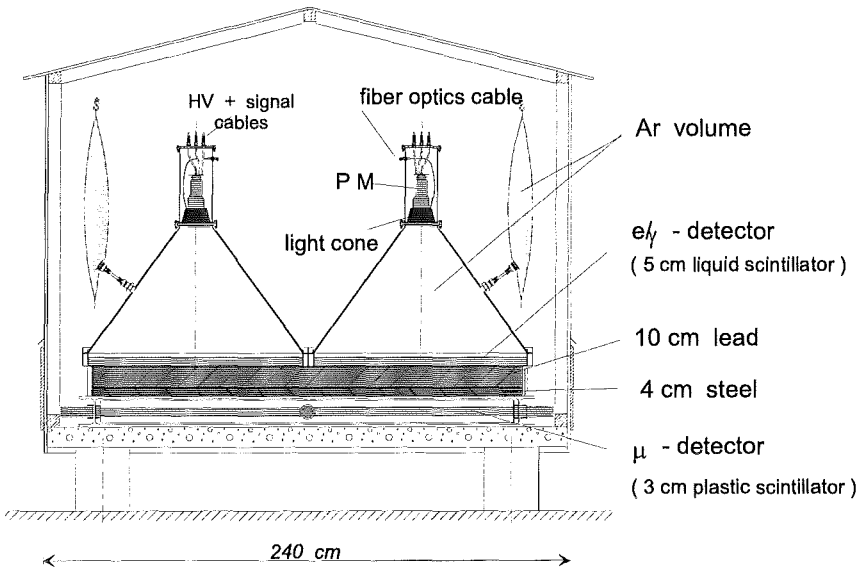

Figure 2: *Schematic view of a detector station of the KASCADE experiment.*

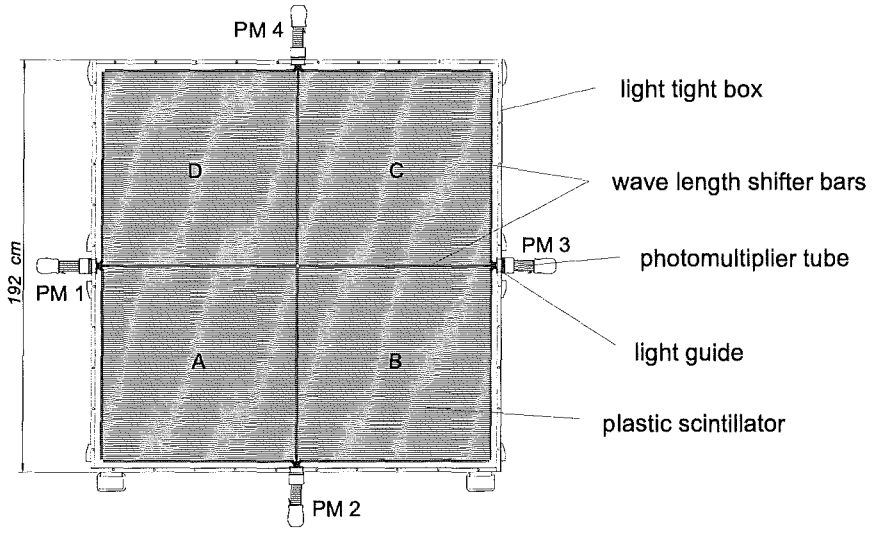

Figure 3: *Muon detector of a station of the KASCADE array.*

outer 12 clusters are additionally equipped with muon detectors. These are four plastic scintillators ($90 \cdot 90 \cdot 3\,\mathrm{cm}^3$ each) placed under absorber material of 10 cm lead and 4 cm iron. The readout is provided by four photomultiplier coupled to the scintillator plates which are connected to each other by wave length shifters (see Figure 3).
In the basement of the central detector, below the last layer of the hadron calorimeter [6], 32 position sensitive multiwire proportional chambers (MWPC) are installed

for the measurements of position and direction of single muons in air showers. The setup (Figure 4) consists of 16 stacks of two chambers one upon another. Each chamber consists of three layers of crossed anode wires and cathode stripes [7]. The crossing angle of the cathodes to the anode wires is $\pm 34°$ at each of the three different size types of the chambers. Figure 5 indicates the determination of the position

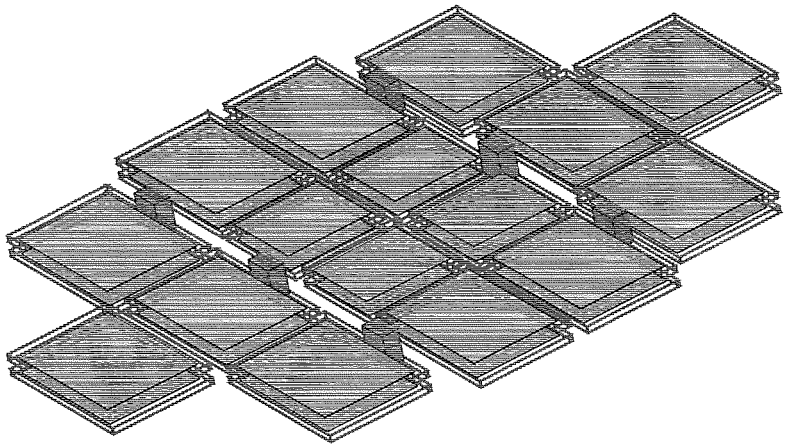

Figure 4: *Two MWPC layers installed in the basement of the central detector.*

of minimal ionisation particles in a single chamber due to the crossing points of wires and stripes. The total sensitive area of the MWPC setup is $2 \times 129\,\mathrm{m}^2$ [8]. The absorber of the calorimeter effects an energy threshold of 2 GeV for vertical muons as compared with 250 MeV for the muon detectors of the array.

From the raw data of the muon and e/γ-detectors of the field array the global shower parameters for each single triggered shower are reconstructed. For triggering a multiplicity of at least half of the detector stations at one cluster is required. By comparisons of detector simulations with the measured deposited energy in the detectors local electron and muon densities at each station are deduced. A fit of the Nishimura-Kamata-Greisen function [9] to the local electron

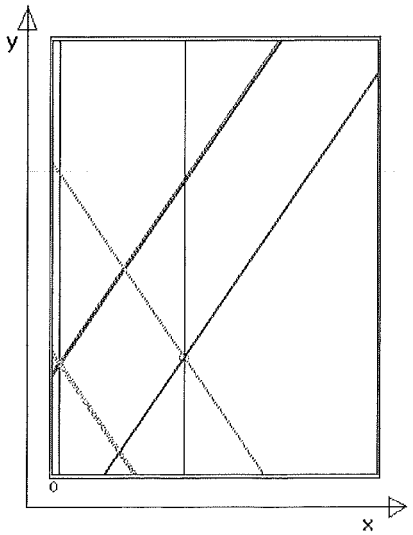

Figure 5: *Anode wires and diagonal cathode strips are used to determine the particle position.*

densities estimates the position of the shower core R and the total number of electrons of the EAS, i.e. the shower size N_e. By measurements of the particle arrival times with the e/γ-detectors the direction of the shower axes (zenith angle Θ and the azimuth Φ) is reconstructed. The so called Greisen function [10] is fitted to the local muon densities and integrated in the range of 40 m$\leq R \leq$ 200 m. The resulting truncated muon number N_μ^{tr} paves to be strongly correlated with the primary energy of the shower, nearly mass independent [11]. The reconstruction accuracy of the shower core is around 1 m - 2.5 m (depending on the shower size), of the arrival direction $\approx 0.3°$, of the shower size N_e ca. 7%, and of N_μ^{tr} ca. 10%.
Muon tracks in the MWPCs are reconstructed using the shower direction. At each stack all combinations of hits of the upper and lower level are compared with the shower direction. Only tracks close to the shower direction are defined with muons. An additional procedure to eliminate δ-electrons produced in the absorber and secondary particles of the punch-through of high-energy hadrons is included [12]. The resulting parameter is the number of reconstructed muons $N_\mu^\star$ with energy higher than 2 GeV observed by the MWPC system for each shower. Additionally the position and direction of each individual muon is deduced. The spatial resolution for the muon reconstruction is $\sigma_x = 0.73$ cm (x is defined as perpendicular to the anode wires) and $\sigma_y = 1.43$ cm (in line of the anodes). Depending on the shower arrival direction the sensitive area of the MWPC system is calculated [13], and thus the local muon density $\rho_\mu^\star$ is estimated. For the reconstruction of the lateral distributions the number of muons and the sensitive area is calculated in core distance rings of a width of 2 m. This procedure is also done for the muons measured with the array stations.

For detailed studies of the detector efficiencies and responses a set of EAS, simulated for the KASCADE observation level (110 m a.s.l.), has been prepared using the Monte Carlo air shower simulation program CORSIKA [14] (Vers.5.6). It includes GHEISHA [15] and different packages of high-energy interaction models like VENUS [16] and QGSJet [17]. The electron-photon component is also simulated by the Monte Carlo procedure of EGS4 [18]. The influence of the Earths magnetic field is taken into account. The calculations cover the energy range of 10^{14} eV - 10^{16} eV for different primary masses.
The response of all KASCADE detector systems to the EAS components has been determined by simulations using the GEANT code [19]. The particles of the generated EAS are tracked with varying core distances from the central detector (up to 100 m). All relevant physical interactions of particles with matter are taken into account, and each produced secondary particle is included in the further tracking procedures. The output of the simulations is stored in the same way as the measured data. Therefore measured and simulated data are reconstructed with the same procedures, thus minimizing systematic errors.

General cuts of the collected data are done on both sets, real data and Monte Carlo to beware systematic errors. Only showers with a reconstructed core inside of an radial distance of 91 m from the middle of the detector array (this is not exactly the position of the central detector) and with shower sizes of $lg(N_e) > 4.5$ and $lg(N_\mu^{tr}) > 3.5$ are included in the further analysis. The size cuts assure that all EAS exceed the mass dependent trigger threshold. Additionally it is selected that all detector components have been in a good operation status. Due to the large computing time of the Monte Carlo procedures, comparisons of simulations with real data distributions are only performed for specific cases.

3 The Lateral Muon Density Distribution

For the determination of the integral lateral distribution of the muon density the shower plane is divided in circular areas centered around the shower axis with a width of $\Delta R = 2\,\mathrm{m}$, summing up the number of muons inside the ring and taking into account the sensitive area. This has been done with a classification of the registered EAS by certain ranges of the values of N_e, N_μ^{tr} and arrival direction. In addition the MLD are dependent on the energy threshold of muon detection ($E_\mu > 250\,\mathrm{MeV}$ for the KASCADE field detectors, $E_\mu > 2\,\mathrm{GeV}$ for the MWPC). Figure 6 shows examples of measured results as compared with simulations. The examples are specified first along a definite range of the shower size, and alternatively with a definite value of the energy indicative quantity N_μ^{tr} ($lgE \propto lg(N_\mu^{tr})$). The limitation of R is due to geometrical restrictions of the detector setup and due to the hadronic and electromagnetic punch-through. For the array detectors core distances of $> 40\,\mathrm{m}$ are necessary to avoid admixture of background, and $> 20\,\mathrm{m}$ for the MWPC system. The data of the MWPC system are corrected for the detection efficiency. A value of 91.7 per cent has been determined as the average during the acquisition period.
The set of simulated showers, used for comparison and studies of the sensitivity to

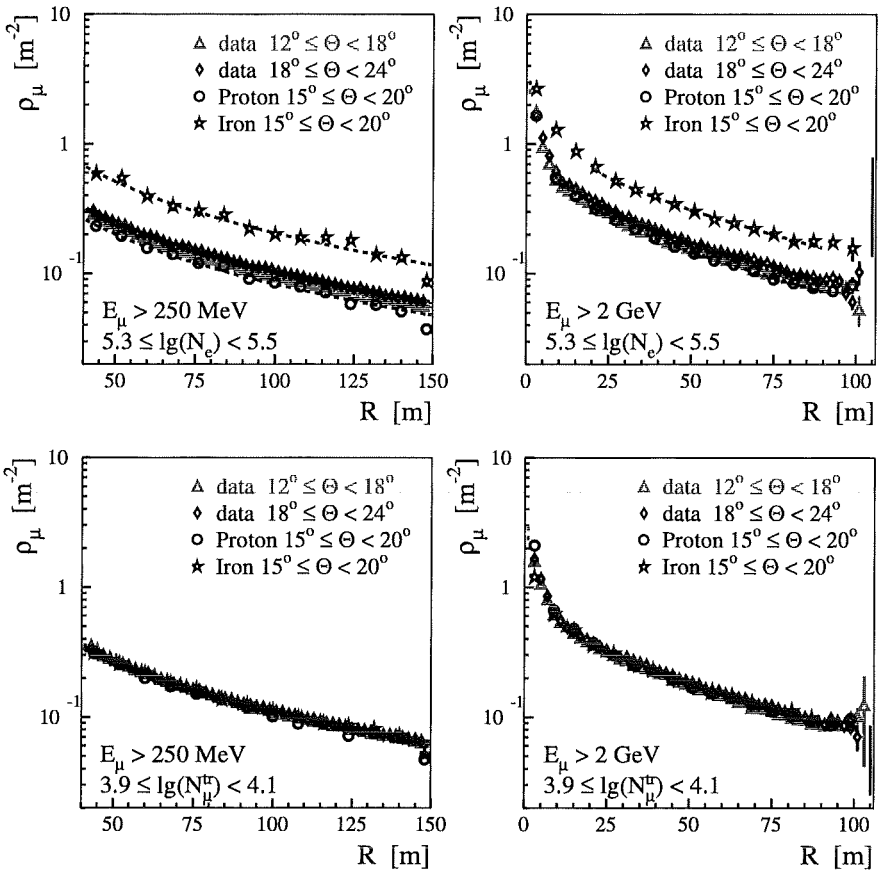

Figure 6: *Measured and simulated lateral muon density distributions for two different energy thresholds of muon detection and classified with a particular range of N_e and N_μ^{tr}, respectively.*

the primary mass, comprises 2000 showers for proton and iron primaries, generated with the QGSJet model for the hadronic interaction and incident with zenith angles between 15° and 20°. For the inclusion of the detector response qualities the simulated showers have been used six times for the detector simulations.
When inspecting Figure 6 we have to recall: (i) In an EAS sample of a defined $lg(N_e)$ range, the EAS-subsample induced by the heavier primaries originates generally from higher primary energies with larger muon intensity. However, due to the rapidly falling primary energy spectrum (and additionally due to the larger fluctuations) the observed sample is dominated by the light primaries. Thus the experimental average lateral muon distribution follows nearly the proton case. (ii) Alternatively classifying the EAS sample by the $lg(N_\mu^{tr})$, obviously the muon content and distributions do not differ significantly - as predicted for the considered lateral range. Due to different interaction lengths of light and heavy primary induced showers the electron-photon component develops differently in both cases, with the effect that in such a sample the iron induced EAS display N_e-values with a factor of 2-3 smaller than proton induced showers observed at sea level [20]. The findings shown in Figure 6 support the concept of the KASCADE experiment to use N_e in a sample of fixed N_μ^{tr} as signature for the primary mass composition.

For the description of the muon lateral distribution (MLD) by a functional form and following the results of ref. [21] the so-called Hillas function

$$\rho_\mu[m^{-2}] = C \cdot \left(\frac{R}{r_0}\right)^{-\beta} \exp\left(\frac{-R}{r_0}\right)$$

has been adopted, introducing different r_0-values for the two different detection thresholds ($r_0 = 600\,\mathrm{m}$ for $E_\mu > 250\,\mathrm{MeV}$, $r_0 = 100\,\mathrm{m}$ for $E_\mu > 2\,\mathrm{GeV}$). This form is used for all lateral distributions with a two-parameter fit of the slope parameter β and a scale parameter $A \equiv \rho_\mu(50)$, the muon density at a core distance of 50 m, $C = A \cdot (r_0/50)^\beta \cdot exp(50/r_0)$.

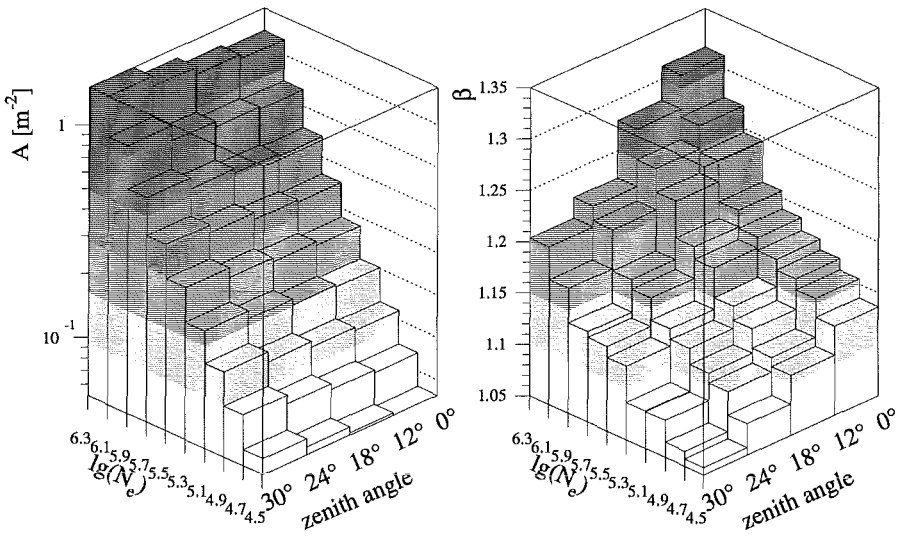

Figure 7: *N_e- and zenith angle- variation of the parameters A and β of the Hillas form fitted to the MLD, measured with $E_\mu > 250\,MeV$.*

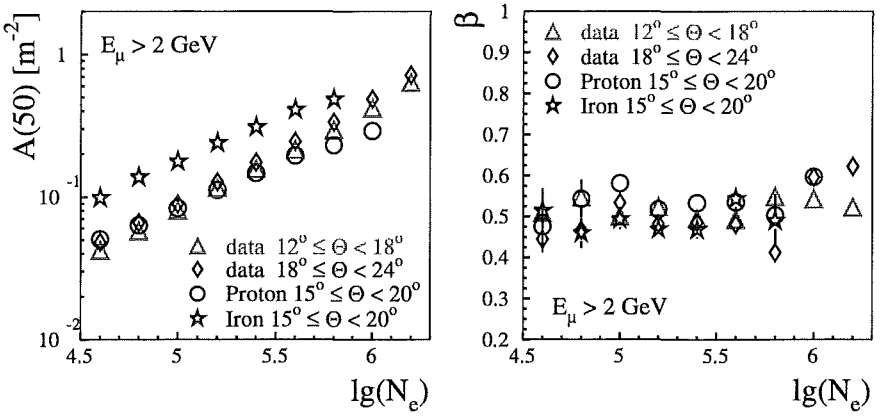

Figure 8: *N_e-variation of the parameters A and β of the Hillas form fitted to the MLD, measured with $E_\mu > 2$ GeV compared with distributions from Monte Carlo simulations.*

Figures 7 and 8 display the variation of the adjusted parameters with the shower size. In Figure 8 some exploratory comparisons with the expectations from the EAS simulations are made. With increasing N_e, and consequently the average primary energy, the shower maximum is reached deeper in the atmosphere, thus producing steeper lateral distributions with larger intensities of the secondaries. In observations with larger zenith angles, however the shower maximum gets more distant from the observation level. Therefore the distributions become flatter and the muon intensity gets larger as the comparative N_e has been lowered by the increased atmospheric absorption of the electron-photon component. Since the higher-energy muons originate from early interactions in the atmosphere, the distributions become flatter with an increased detection threshold. The intensity is naturally decreased in this case. With the same argumentation we understand the flatter MLD, with larger intensities predicted for the heavy primaries, and the reduced steepening for larger detection thresholds.

4 $N_\mu - N_e$ Correlation

A powerful mass-sensitive EAS observable, measured in air shower investigations, is the correlation of the muon content N_μ with the shower size N_e [22, 23]. The full muon content N_μ, however, is a quantity hardly accessible experimentally. In recent KASCADE studies [5] the muon size is represented by the quantity N_μ^{tr}, and the N_e/N_μ^{tr}-ratio is evaluated for each single shower event and the mean value and its fluctuations are subsequently determined for the studied range of N_μ^{tr} or N_e. In many other experiments (MSU [24], Tien-Shan [25], Akeno [26]), due to the low muon densities and muon detectors of insufficient size, the muon content, averaged over many observed showers and correlated with the (average) N_e is used for studies of the mass composition signatures. The experimental KASCADE results about the integral MLD, presented in the preceding section, allow to follow this concept of evaluating the correlation and to compare this with the single event determination. In order to proceed in this way and to avoid questionable extrapolations of the form of the lateral muon distribution to large distances, the MLD, parameterized by the Hillas form and fitted to the data, are integrated in the range limited to $40 - 100$ m from the shower center. The variation of this quantity N_μ^{100} with the shower size are studied for two different muon detection thresholds. Results and simulation predictions are shown in Figure 9. The variation can be described by a power-law dependence $N_\mu^{100} \sim (N_e)^\gamma$ whose indices are given in Table 1.

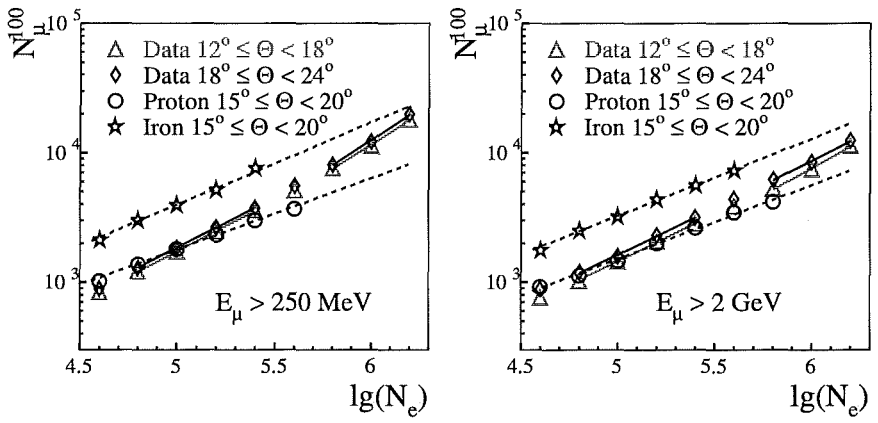

Figure 9: *The $N_\mu - N_e$ correlation of the data for different muon detection thresholds compared with Monte Carlo simulations. The lines represent fits by a power-law dependence.*

For the data the exponent shows a significant change in the value from γ_1 to γ_2 at the N_e-value which is indicated as knee in the N_e spectrum observed by the KASCADE measurements [5]. Regarding Figure 9 the simulation results for large N_e values are not very accurate due to a too small number of simulated EAS. It should be also noted that the significant difference between simulations and the first data point can be understood in terms of the N_e fluctuations from EAS of lower primary energies (lower than included in the simulations) with smaller muon contents.

The possibility of the KASCADE detector system to measure the average muon content of EAS with two different energy thresholds lets us introduce a further EAS parameter: the ratio of the integrated number of muons above two different

data		zenith angle			
		$0° \leq \Theta < 12°$	$12° \leq \Theta < 18°$	$18° \leq \Theta < 24°$	$24° \leq \Theta < 30°$
$E_\mu >$ 250 MeV	γ_1	0.78 ± 0.02	0.79 ± 0.02	0.78 ± 0.02	0.79 ± 0.02
	γ_2	0.92 ± 0.03	0.94 ± 0.03	0.97 ± 0.03	0.98 ± 0.03
$E_\mu >$ 2GeV	γ_1	0.73 ± 0.03	0.73 ± 0.02	0.70 ± 0.02	0.70 ± 0.02
	γ_2	0.77 ± 0.04	0.83 ± 0.03	0.74 ± 0.04	0.77 ± 0.03
simulation		zenith angle $15° \leq \Theta < 20°$			
		proton		iron	
$250MeV$	γ	0.57 ± 0.04		0.64 ± 0.04	
$2GeV$	γ	0.57 ± 0.02		0.60 ± 0.04	

Table 1: *Exponents γ of the power law description $N_\mu^{100} \sim (N_e)^\gamma$. The quoted errors arise from the fits of the MLD to the data. The exponents γ_1 and γ_2 describe the slopes before and after the knee position, as observed in the N_e spectrum by the KASCADE experiment at $lgN_e^{knee} = 5.65$ (at $\Theta = 20°$).*

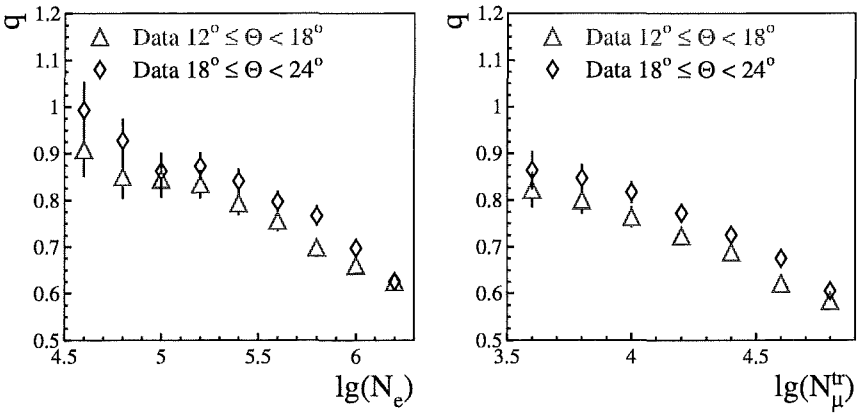

Figure 10: *The variation of the ratio of the average muon contents with two different muon detection thresholds: $q = N_\mu^{100}(2\,GeV)/N_\mu^{100}(250\,MeV)$, with $lg(N_e)$ and $lg(N_\mu^{tr})$.*

values of E_μ. It is shown by the variation of $q = N_\mu^{100}(2\,\mathrm{GeV})/N_\mu^{100}(250\,\mathrm{MeV})$ with $lg(N_e)$ and $lg(N_\mu^{tr})$, respectively in Figure 10. The observable q is sensitive to the energy spectrum of the secondaries produced during the shower development. The decrease of q with the shower size and N_μ^{tr} (primary energy) can be qualitatively explained by the increased chance of the lower energy muons to reach the observation level. Similarly the dependence on the zenith angle of incidence is understood. Remarkably the variations (shown in Figure 10) indicate a kink corresponding [5] to knee positions in the N_e and N_μ^{tr} spectrum. Actually, as expected from the different EAS development, CORSIKA simulations reveal some mass sensitivity of q with larger values for the heavy primary induced EAS. However, including the detector responses the effects get smeared out within the actual statistical accuracy.

5 Muon Density Fluctuations

The EAS muon density and its fluctuations, locally measured at fixed distances from the shower center carry interesting information about energy and nature of the primary [22]. As already stressed, in an EAS sample classified along the shower size N_e the heavy primary induced EAS have systematically higher energies and consequently higher muon densities. Simultaneously in a sample of definite energy (approximately selected with a definite N_μ^{tr} value in case of the KASCADE detector) light-particle induced EAS are expected to show larger fluctuations of the shower observables. In order to work out these features for the density distributions of EAS muons, we analyse the local muon densities ρ_μ^*, measured at a particular distance R from the shower core by use of the MWPC system of the KASCADE central detector. The measured EAS are selected for a zenith angle range of $15° \leq \Theta \leq 20°$ and core distance $30\,\mathrm{m} < R < 50\,\mathrm{m}$. This choice is a compromise between the Θ- and R- variation of the muon density and a sample size of statistical significance of the results (see ref. [27]).

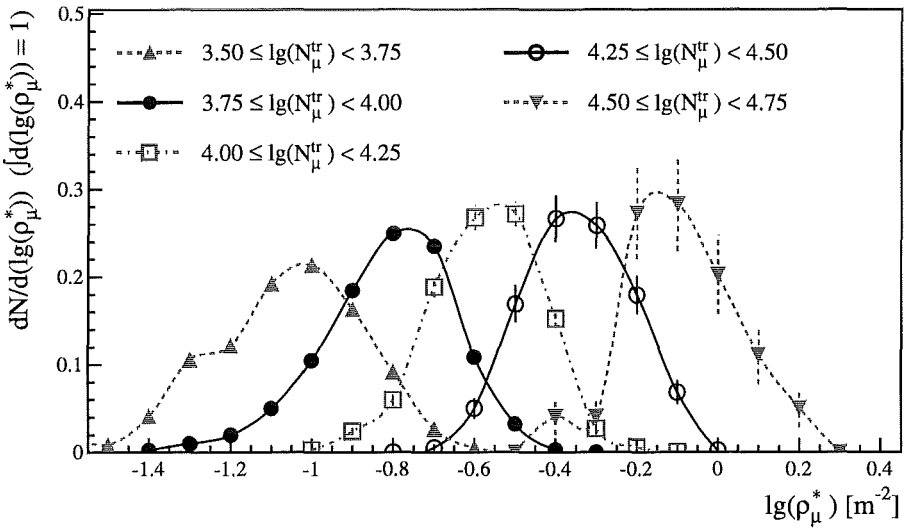

Figure 11: *Distributions of local muon densities ($E_\mu > 2\,GeV$, $30\,m \leq R \leq 50\,m$, $15° \leq \Theta \leq 20°$) of shower groups of different ranges of $lg(N_\mu^{tr})$. For guiding the eyes the symbols are connected by smooth lines.*

Figure 11 shows the measured ρ_μ^* distributions for five ranges of N_μ^{tr} ($\propto$ primary energy). The lower two ranges are below, the upper two above the knee in the N_μ^{tr}-spectrum, which is ascribed to $lg(N_\mu^{tr}) \approx 4.1$ [28]. The mean of ρ_μ^* is increasing with N_μ^{tr} as expected for larger energies and with increasing primary energy the fluctuations of the muon density decrease.
The muon densities grouped by the shower size N_e are shown in Figure 12. As expected the muon densities are increasing with larger N_e, but reduced widths (fluctuations) of the distributions are not observed. Since N_e is mass dependent in contrast to N_μ^{tr}, the showers of the sample with larger primary mass have a larger local muon density due to the larger primary energy at the same shower size. Consequently the broading of the distributions in Figure 12 result mainly from the mixture of different masses, and not from intrinsic shower fluctuations.

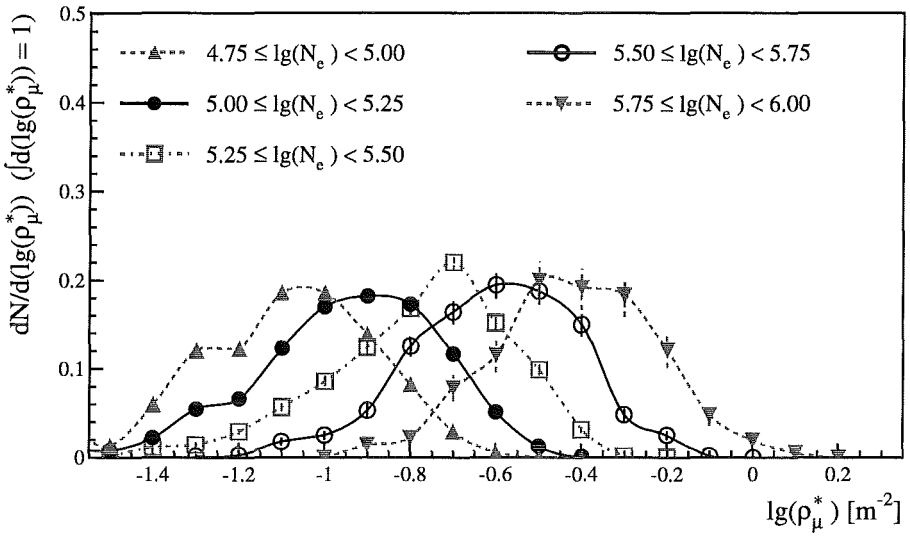

Figure 12: *Distributions of local muon densities ($E_\mu > 2\,GeV$, $30\,m \leq R \leq 50\,m$, $15° \leq \Theta \leq 20°$) of shower groups of different ranges of $lg(N_e)$. For guiding the eyes the symbols are connected by smooth lines.*

In order to clarify this point, some distributions shown in Figures 11 and 12 are compared with predictions from simulations (see Figure 13). Shower samples grouped in N_μ^{tr} ($E_\mu > 250\,\mathrm{MeV}$), display negligible differences in the mean and in the width of the local muon density distribution ($E_\mu > 2\,\mathrm{GeV}$) between proton and iron induced showers at around 40 m core distance (Figure 13 left side). In the highest energy range a slight distinction gets visible. For comparisons of Monte Carlo results and data with one-dimensional distributions a parametrisation of a Gauss-function of the natural logarithmic of the observables is often useful. The presented results show that the observed distributions do not follow a Gaussian distribution. When grouping the showers by N_e there appear differences in the mean and the width of the distributions between the simulated proton and iron induced showers (Figure 13 right side). The general enhancement of light primary induced showers in samples of equal shower size obscures the effect. Nevertheless there appears slight shifts of the measured distributions in direction to the iron distribution with increasing shower sizes.

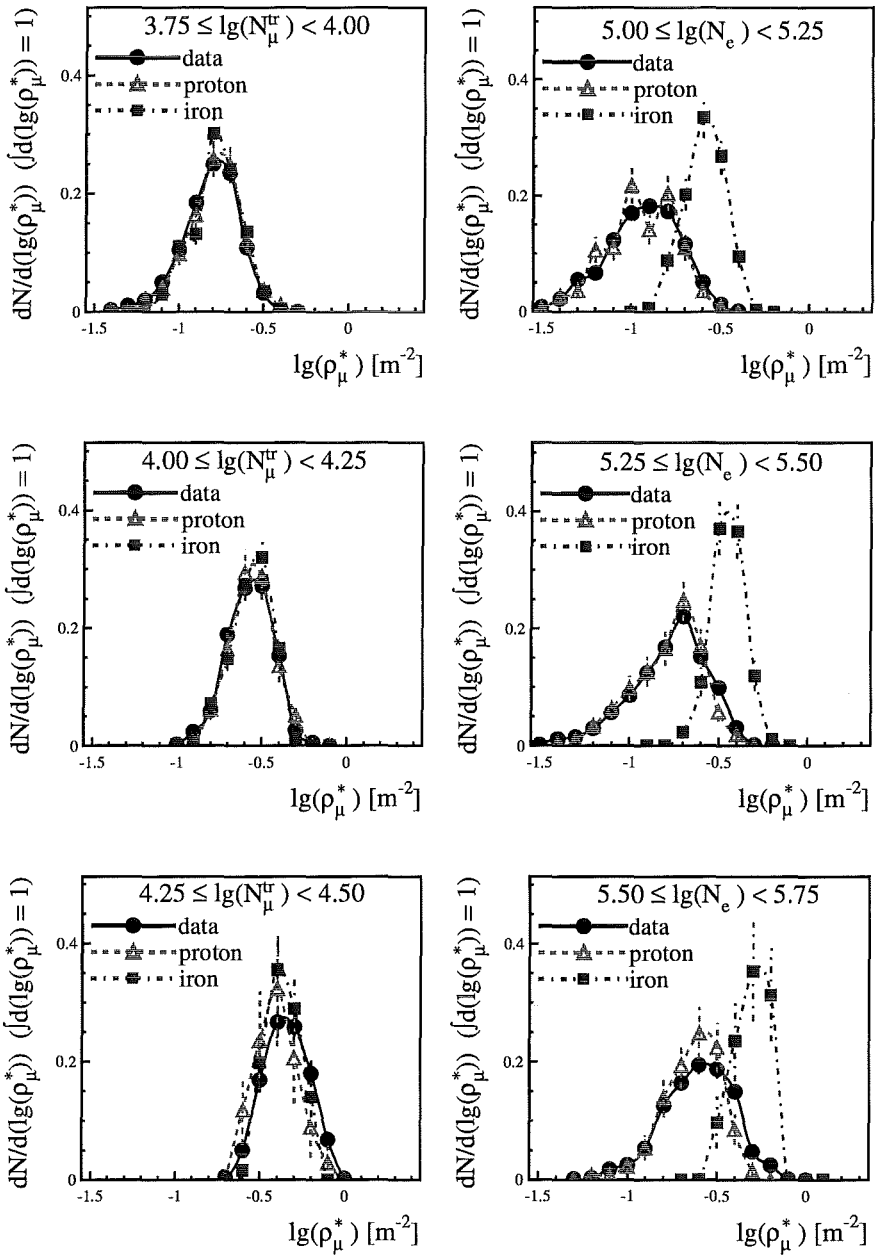

Figure 13: *Comparisons of measured local muon densities ($E_\mu > 2\ GeV$, $30\,m \leq R \leq 50\,m$, $15° \leq \Theta \leq 20°$) with simulated distributions for ranges in N_μ^{tr} (left) and N_e (right). For guiding the eyes the symbols are connected by smooth lines.*

6 Muon Density Spectrum

In addition to the lateral distribution and the fluctuations of the local muon density ρ_μ^* of well specified showers, the spectrum of ρ_μ^* of the EAS observed in a certain distance from the shower core and for a certain range of the angle of shower incidence is a quantity of considerable interest. Figures 14 and 15 display integral muon density spectra measured with the MWPC system ($E_\mu > 2\,\mathrm{GeV}$) for two particular core distances and for the zenith angle range $10° \leq \Theta \leq 30°$. The effective data aquisition time was 263 days. The spectra follow a power law form $dN/d\rho_\mu^* \propto (\rho_\mu^*)^{-\beta}$. Plotting the spectra with multiplying the muon density by $(\rho_\mu^*)^{2.3}$ reveals a kink in the spectra, similar to the knee in the N_e and N_μ distributions, expressed by the change of the spectral index β. For the shown examples the kinks happen at $\rho_\mu^* = 0.26\,\mathrm{m}^{-2}$ and $\rho_\mu^* = 0.18\,\mathrm{m}^{-2}$, respectively, with a change of $\beta_1 = 3.33 \pm 0.01$ before the knee to $\beta_2 = 3.67 \pm 0.21$ after the knee for the shower core distance of $40 - 45\,\mathrm{m}$, and from $\beta_1 = 3.41 \pm 0.01$ to $\beta_2 = 3.71 \pm 0.05$ for the shower core distance of $65 - 70\,\mathrm{m}$. The quoted errors represent the statistical uncertainties. Due to the reduced efficiency of the trigger threshold for small sized showers the first data points in Figure 14 have not been included in the fit procedure. With increasing distance from the shower core the position of the kink shifts to lower muon densities as a consequence of the lateral distributions of the EAS muons of decreasing muon densities with increasing R. This explains also the steeper slopes of the density spectra at larger R.

In order to analyse these results and to relate the local muon densities to the energy and nature of the primaries detailed Monte Carlo calculations simulating the EAS development have been performed. Using the CORSIKA code [14] samples of proton and iron induced EAS of the energy range of $5 \cdot 10^{14}\,\mathrm{eV}$ to $1 \cdot 10^{16}\,\mathrm{eV}$, distributed along a primary energy spectrum $\propto E^{-2.7}$ are generated with two different interaction models (QGSJet and VENUS). The detector efficiency has been included in the simulations, using each simulated EAS ten times in the considered ranges of the core distance.

Figure 16 displays the relations between the average muon density ρ_μ^* and the primary energy, described by a power law $\rho_\mu^* \propto E^\delta$. The values of δ resulting from

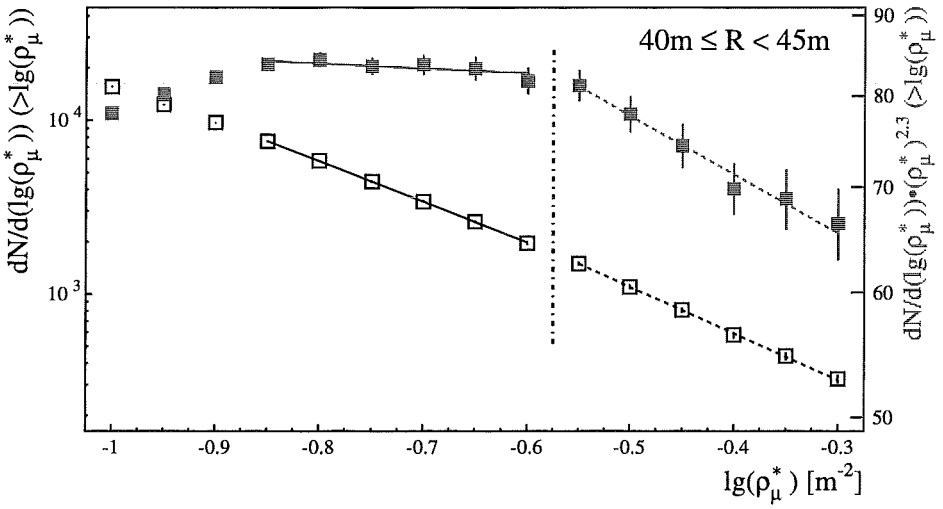

Figure 14: *Integral muon density spectrum measured by the MWPC for showers with a core distance of* $40\,m \leq R \leq 45\,m$ *(left scale). The same spectrum multiplied by* $(\rho_\mu^*)^{2.3}$ *makes the change in the index visible (right scale). The vertical line assigns the position of the knee in the muon density spectra.*

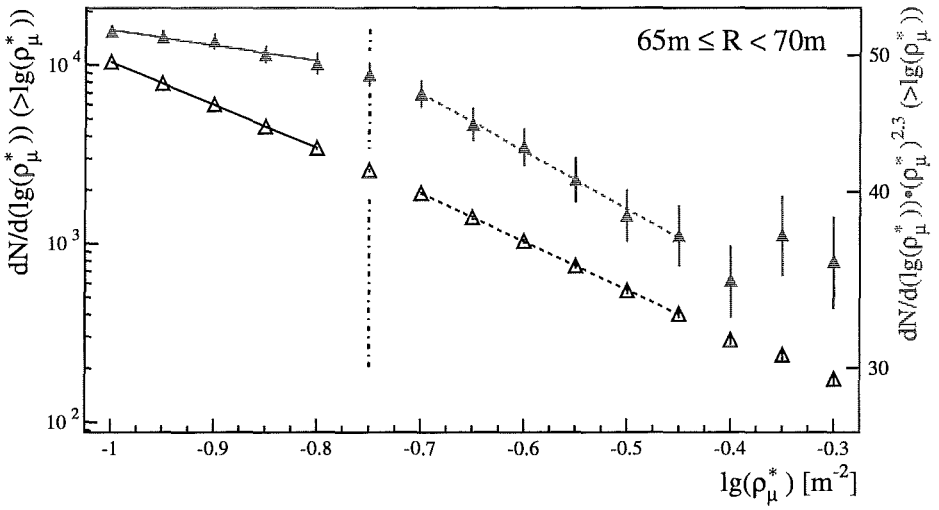

Figure 15: *Integral muon density spectrum measured by the MWPC for showers with a core distance of* 65 $m \leq R \leq$ 70 m *(left scale). The same spectrum multiplied by* $(\rho_\mu^*)^{2.3}$ *makes the change in the index visible (right scale). The vertical line assigns the position of the knee in the muon density spectra.*

a fitting procedure are listed in Table 2. The quoted uncertainties are due to the limited statistics of the simulated showers. On basis of these results the position of the knee in the muon density spectra and the spectral indices β are related to the knee position and the index γ of the energy spectrum $dN/dE = dN/d\rho_\mu^* \cdot d\rho_\mu^*/dE$

	δ (QGSJet)		δ (VENUS)	
	proton	iron	proton	iron
40 m$\leq R \leq$ 45 m	0.718 ± 0.015	0.807 ± 0.009	0.776 ± 0.016	0.784 ± 0.010
65 m$\leq R \leq$ 70 m	0.727 ± 0.017	0.809 ± 0.012	0.811 ± 0.015	0.763 ± 0.012

Table 2: *Exponents of the power law function* $\rho_\mu^* \propto E^\delta$ *for different core distances, primaries and high-energy interaction models.*

	proton	iron
	QGSJet	
γ_1	$2.71 \pm 0.01_{stat} \pm 0.38_{sys}$	$2.92 \pm 0.01_{stat} \pm 0.27_{sys}$
γ_2	$2.95 \pm 0.04_{stat} \pm 0.46_{sys}$	$3.18 \pm 0.04_{stat} \pm 0.34_{sys}$
E_{knee}	$(7.27 \pm 0.43_{stat} \pm 2.33_{sys}) \cdot 10^{15}$ eV	$(4.56 \pm 0.10_{stat} \pm 1.10_{sys}) \cdot 10^{15}$ eV
	VENUS	
γ_1	$2.88 \pm 0.01_{stat} \pm 0.27_{sys}$	$2.83 \pm 0.01_{stat} \pm 0.25_{sys}$
γ_2	$3.14 \pm 0.04_{stat} \pm 0.35_{sys}$	$3.08 \pm 0.05_{stat} \pm 0.32_{sys}$
E_{knee}	$(5.34 \pm 0.24_{stat} \pm 1.36_{sys}) \cdot 10^{15}$ eV	$(4.60 \pm 0.21_{stat} \pm 0.99_{sys}) \cdot 10^{15}$ eV

Table 3: *Spectral indices* γ_i *of the primary energy spectrum, obtained with different high-energy interaction models and primary particles. Additionally the estimated position of the knee is given. Sources of the errors are given in the text.*

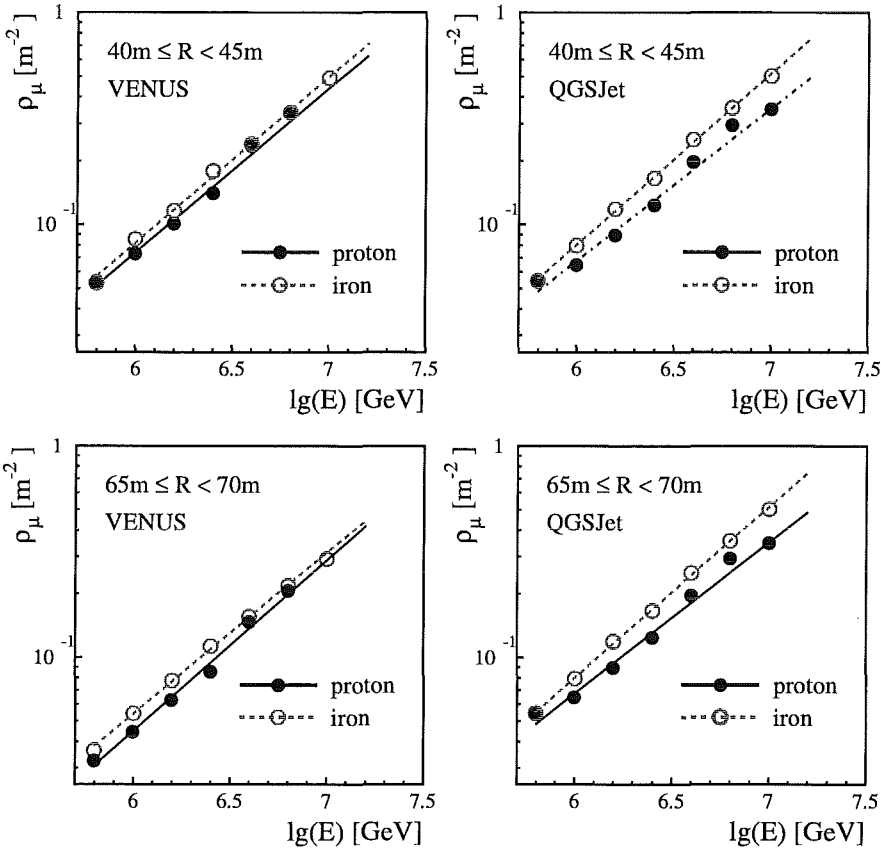

Figure 16: *Dependence of the local muon density on the primary energy for two different ranges of core distances, for two different primaries, and for two high-energy interaction models of the CORSIKA simulations with full detector simulation included.*

leading to $\gamma = \delta \cdot (\beta - 1) + 1$.
The results of this procedure are given in Table 3. Sources of the systematic uncertainties for the values of the knee position are the evaluation of the position of the kink in the measured muon density spectra ($\pm 0.015\,\mathrm{m}^{-2}$), the variation of the observed density within the core distance interval of 5 m ($\pm 0.01\,\mathrm{m}^{-2}$) and the uncertainty in the estimate of δ (see Table 2).
The systematic uncertainties of the spectral indices γ have the following sources:
• The value of δ has an uncertainty of $\approx \pm 0.1$ due to the multiple use of single showers in the detector simulation.
• The index β of the muon density spectra has an estimated inaccuracy of ± 0.01 for β_1 and ± 0.12 for β_2 as a result of the considered width of the bins of the core distance.
• the azimuthal asymmetry of the MWPC setup leads to an additional uncertainty of β by ± 0.06 and ± 0.15.
• The range of the data for fitting the exponent β depends on the trigger threshold, on statistics and on the knee position. This leads to an uncertainty in β of ± 0.01.
The fluctuations of $\rho_\mu^\star$ lead to an additional (not included) uncertainty of the spectral indices, which would shift the γ_2 to a slightly increased value.

7 Concluding Remarks

Using the KASCADE detector facilities detailed measurements of the EAS muon density and its fluctuations have been performed at two different muon energy detection thresholds, and classified according to the EAS size and the energy indicative parameter N_μ^{tr}, average lateral muon density distributions have been determined. In addition, in fixed distances from the shower center muon density spectra have been measured. The observed features, and in particular the sensitivity to the mass composition, are studied in context of CORSIKA simulations, based on different models of the high-energy hadronic interaction. Special attention is payed to conspicuities of the variations of the observed quantities which may be related to the slopes and the knee in the EAS size spectrum or possible changes in the mass composition. The main results are the following:

• The lateral muon density distributions are well described in the observed radial ranges by a Hillas form, specified by a slope parameter β and an intensity scaling parameter A. The variation of these parameters with $lg(N_e)$ can be generally understood from known features of longitudinal shower development, and comparisons with simulations of proton and Fe induced showers indicate a change, in particular of the intensity scaling parameter for $lg(N_e) \approx 5.6$. However, a quantitative mass discrimination is hampered by the dominance of light particle induced EAS in groups classified along N_e.

• By integrating the lateral distributions from $40-100$ m an experimentally accessible quantity N_μ^{100}, representing the muon content, is introduced for a consideration of the N_e - N_μ correlation. For both muon detection thresholds the variation of N_μ^{100} with N_e displays a significant change of the slopes at the knee, pointing to a heavier composition. The changes of the indices of the power law dependence of N_μ^{100} are consistent with similar observations around the knee of other experiments [29, 30].

• It should be stressed that - in contrast to recent applications of the $N_e - N_\mu$ correlation method by an event-by-event analysis - the present studies do relate average quantities. The results imply a consistency check and confirm previous KASCADE results and observed tendencies.

• A quantity of special interest is the ratio $q = N_\mu^{100}(2\,\mathrm{GeV})/N_\mu^{100}(250\,\mathrm{MeV})$ of the number of muons detected with different thresholds. This ratio is not only sensitive to the number, but also to the energy spectrum of the produced secondaries and could also help to test the ingredients of Monte Carlo simulations. The observed variations of q exhibit clearly a change in the slope where the knee position is determined by recent KASCADE results.

• It is known that the EAS muon density and its fluctuations, locally measured at fixed distances from the shower center carry information about the primary, which could replace the information from observations of the lateral distributions and muon numbers from integration over a larger radial ranges [2, 31]. Distributions of the muon density have been measured for fixed ranges of distances from the shower center and classified by the EAS size and N_μ^{tr}, respectively. The broad distributions, which do not follow logarithmic Gauss distributions, could be compared with Monte Carlo simulations in order to explore mass discrimination effect. The data exhibit the dominance of light particle induced showers in N_e-classified groups, and the simulations predict an insignificant mass discrimination in N_μ^{tr}-classified groups.

• A result of considerable interest is the first observation of kinks in muon density spectra measured at fixed distances from the shower core. Adopting a particular mass composition and invoking Monte Carlo simulations (by CORSIKA), the kinks and slopes of the density spectra can be related to the knee position and spectral indices of the primary energy spectrum. The resulting indices are about -2.8 before and about -3.1 after the knee position of about $5 \cdot 10^{15}$ eV. This is in good

agreement with other measurements (the CASA-MIA result [32] e.g.) and a most recent event-by-event analysis of the KASCADE data applying advanced statistical methods and decision criteria [33].
Thus we may summarize that after the evidence for the existence of the knee discontinuity in the N_e spectrum by Kulikov and Khristiansen [1] and many other subsequent experiments (see ref. [2]), lateron in the spectrum of the EAS muon content [34, 5] and recently in the hadron number by the KASCADE group [35], also the muon density is shown to reveal consistently the phenomenon.

Finally we note that the present studies of various observables of the EAS muon component point to a change of the chemical compositions to heavier nuclei beyond the knee, in agreement with various other results of analyses of KASCADE data [23]. All analyses, however, invoke comparisons with Monte Carlo simulations on basis of specific hadronic interaction models. The model dependence can be relieved by the constraint of a simultaneous description of various different observables. The observation of the EAS muon densities with high statistical accuracy is contributing in this direction.

Acknowledgments

The communicated results have been obtained in course of the investigations of the KASCADE experiment. The work has been partly supported by a grant of the Romanian Ministery of Research and Technology as well as by a research grant (No.94964) of the Armenian Government and by the ISTC project A116. The collaborating group of the Cosmic Ray Division of the Soltan Institute of Nuclear Studies in Lodz and of the University of Lodz is supported by the Polish State Committee for Scientific Research (Grant No. 2 P03B 160 12). The KASCADE collaboration work is embedded in the frame of scientific-technical cooperation (WTZ) projects between Germany and Armenia (No.002-98), Poland (No.92-94) and Romania (No.RUM-014-97). The authors would like to thank the technical staff of the institute for valuable cooperation.

References

[1] G. V. Kulikov, G. B. Khristiansen, Soviet Physics JETP **35** (1959) 441

[2] N. N. Kalmykov, G. B. Khristiansen, Journal Phys. **G 21** (1995) 1279

[3] M. Giller, Nucl. Phys. (Proc.Suppl.) **52B** (1997) 164

[4] H. O. Klages et al. - KASCADE Collaboration, Nucl.Phys. (Proc.Suppl.) **52B** (1997) 92

[5] H. O. Klages et al. - KASCADE Collaboration, Highlight Talk at the 25th ICRC, Durban, South Africa, World Scientific 1997, eds. M. S. Potgieter, B. C. Raubenheimer, D. J. van der Walt, p. 297

[6] H. H. Mielke et al., Nucl. Instr. Meth. **A 360** (1995) 367

[7] F. Herm et al., Roman. Journ. Physics **38** (1993) 475

[8] A. Haungs et al., Nucl. Instr. Meth. **A 372** (1996) 515

[9] K. Greisen, Progress in Cosmic Ray Physics 3, North Holland Publ. (1956)

[10] K. Greisen, Ann. Rev. Nucl. Sci. **10** (1960) 63

[11] J. Weber et al., Proc. 25th Int. Cosmic Ray Conf., Durban **6** (1997) 153

[12] A. Haungs, FZKA-Report 5845 (in German), Forschungszentrum Karlsruhe (1996)

[13] H. Leibrock, FZKA-Report 6098 (in German), Forschungszentrum Karlsruhe (1998)

[14] D. Heck et al., FZKA-Report 6019, Forschungszentrum Karlsruhe (1998)

[15] H. Fesefeldt, Report PITHA 85/02, RWTH Aachen, Germany (1985)

[16] K. Werner, Phys. Rep. **232** (1993) 87

[17] N. N. Kalmykov and S. S. Ostapchenko, Yad.Fiz. **56** (1993) 105

[18] W. R. Nelson, H. Hiroyama, D. W. O. Rogers, SLAC Report 265 (1985)

[19] GEANT: CERN Program Library Long Writeups W5013 (1993)

[20] J. Knapp, FZKA-Report 5970 (in German), Forschungszentrum Karlsruhe (1998)

[21] H. Leibrock, A. Haungs, H. Rebel, FZKA internal report (in German), Forschungszentrum Karlsruhe (1998), unpublished

[22] P. R. Blake, W. F. Nash, J. Phys. G: Nucl. Part. Phys. **24** (1998) 217

[23] J. Knapp, Rapporteur Talk at the 25th ICRC, Durban, South Africa, World Scientific 1997, eds. M. S. Potgieter, B. C. Raubenheimer, D. J. van der Walt, p. 83

[24] G. B. Khristiansen et al., Proc. 15th ICRC, Plovdiv **8** (1977) 148

[25] T. V. Danilova et al., Proc. 17th ICRC, Paris **6** (1981) 146

[26] T. Hara et al., Proc. 18th ICRC, Bangalore **11** (1983) 281

[27] K. U. Köhler, FZKA-Report 6214 (in German), Forschungszentrum Karlsruhe (1998)

[28] R. Glasstetter et al., Proc. 16th Eur. Cosmic Ray Symp., Madrid H.E. 7.4 (1998)

[29] T. V. Danilova et al., Proc. 24th ICRC, Rome **1** (1981) 286

[30] C. Chakrabarti et al., Proc. 24th ICRC, Rome **1** (1981) 387

[31] P. R. Blake, W. F. Nash, J. Phys. G: Nucl. Part. Phys. **21** (1995) 1731

[32] M. A. Kennedy Glasmacher, Ph.D.-Thesis, University of Michigan, unpublished

[33] M. Roth, FZKA-Report 6262 (in German), Forschungszentrum Karlsruhe (1999)

[34] J. N. Stamenov et al., Trudy FIAN SSSR **109** (1979) 132

[35] J. Hörandel et al., Proc. 10th ISVHECRI, Assergi, Italy 1998, Nucl. Phys. B (Proc.Suppl.) (in press)